Journal of the Iranian Chemical Society (2022) 19:463–473
https://doi.org/10.1007/s13738-021-02322-9

ORIGINAL PAPER

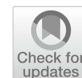

Electrochemical investigation of di-phosphonic acid on corrosion inhibition behavior of copper in hydrochloric acid medium

Naima Sait[1] · Nabila Aliouane[1] · Nadia Ait Ahmed[1] · Mousa Al-Noaimi[2]

Received: 17 October 2020 / Accepted: 18 June 2021 / Published online: 26 June 2021
© Iranian Chemical Society 2021

Abstract

The inhibitory performance of the Methylene bis[(2-hydroxy-5,1-phenylene)methylene] bis phosphonic acid (DPA) on corrosion of copper in 0.5 M HCl has been studied experimentally and theoretically. The inhibition was investigated by electrochemical tests (electrochemical impedance, potentiodynamic polarization), weight loss methods and surface morphology analysis. The parameters obtained by density functional theory (DFT) were calculated and discussed. Impedance spectroscopy results showed that the R_t values are increased but the values of CPE are decreased with decrease in DPA concentration. Potentiodynamic polarization measurements indicate that DPA inhibits both the anodic and cathodic reactions of copper. Thus, they refer to the mixed-type corrosion inhibitor. The adsorption of inhibitor on the copper surface follows Frumkin adsorption isotherm. Scanning electron microscopy (SEM) and X-ray diffraction (XRD) showed that DPA forms a dense film on the copper surface. The results obtained showed that DPA reveals good anti-corrosion capacity.

Keywords Copper · Hydrochloric acid · Corrosion inhibitor · Electrochemical methods · DFT · Frumkin adsorption

Introduction

Hydrochloric acid solutions are one of the most corrosive media. Therefore, investigating the inhibitory performance of copper corrosion in this acid solution is important for academia and industrial [1]. Copper equipment can be easily corroded by hydrochloric acid media which is used to dissolve the corrosion products [2]. Organic inhibitors are commonly used to protect copper from corrosion [3–17]. The organophosphorus compounds and their phosphonate derivatives are particularly among the best inhibitors used because they are non-toxic, water soluble and prepared in a high purity and with low cost [18–20].

A previous study demonstrated that compounds which have phosphonate acid PO_3H_2 group connected with aromatic spacer are effective inhibitors to protect carbon steel and copper from corrosion [21–23]. The presence of (PO_3H_2) and benzene rings in their structure produces more than one center for chemical adsorption and forms a stable adsorption layer on the metal.

Previously, complexing power of two polyphosphonic acid ligand namely {Methylenebis [(2-hydroxy-5,1,3-phenylene)bismethylene]} tetraphosphonic acid (TPA) and {[2-hydroxy-5(4-hydroxybenzyl)-1,3-henylene] bis (methylene)} bisphosphonic (DPA) (Scheme 1) for Cu^{2+} and Fe^{3+} cations was tested to obtain the stability constant [24]. We found that the stability constants of DPA-Cu and DPA-Fe are superior to those obtained with TPA. Because of this, in the present study, we expect that DPA will be a good inhibitor to protect copper from corrosion. The inhibition efficiency and corrosion rate will be investigated by polarization curves, weight loss electrochemical impedance spectroscopy (EIS). Scanning electron microscopy (SEM) and X-ray diffraction (XRD) will be used to describe the morphology and the surface roughness of the uninhibited and inhibited copper samples. The DFT calculations will be used to verify the mechanism of Cu corrosion.

✉ Nabila Aliouane
nabila_aliouane@yahoo.fr

[1] Laboratoire D'Electrochimie, de Corrosion Et de Valorisation Energétique, Département de Génie Des Procédés, Université de Bejaia, Bejaïa, Algeria

[2] Department of Chemistry, Hashemite University, P.O. Box 150459, Zarqa 13115, Jordan

Scheme 1. Chemical molecular structure of DPA and TPA

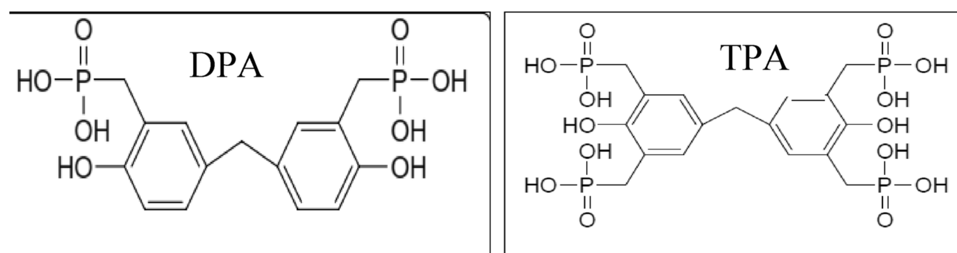

Experimental work

Electrochemical, scanning electron microscopy (SEM) and X-ray diffraction (XRD) tests

The metal used for the current study was copper having 99.9% purity. 0.5 M HCl was prepared by diluting the analytical grade 36–38% HCl with distilled water. The inhibitor {Methylene dis [(2-hydroxy-5,1-phenylene) methylene]} bisphosphonic acid (DPA) was synthesized according to the published procedure [25]. The concentration of the inhibitor was investigated in the range 10^{-5}–10^{-9} M.

Copper samples for weight loss studies were rectangular in size (3 × 1 × 0.1 cm). The copper was polished with a series of emery paper (grade 600–800–1200) and then washed with distilled water and acetone. The test samples were immersed totally in a 50-ml beaker that has 0.5 M of HCl and different concentrations of DPA for 1 h. Three-electrode system consists of copper working electrode (WE), platinum grid as the counter electrode (CE) and a saturated calomel electrode (SCE) as the reference electrode (RE), which was used in all experiments. The electrochemical impedance measuring signal was a sine wave ranging from 100 kHz to 10 mHz. Polarization experiment was conducted by varying the concentration of the inhibitor at a scan rate of 10 mV/s in the range – 1.5 to 1.5 V. The experiments were repeated approximately four times to guarantee reproducibility. The morphology and chemical composition of the inhibited and uninhibited samples were examined using scanning electron microscopy (SEM) and X-ray diffraction (XRD), respectively.

Quantum chemical calculations

Full geometry optimization of DPA was carried out using density functional theory (DFT) at the B3LYP level [26]. All calculations were carried out with the Gaussian 09 program package [27]. The geometry optimization of DPA and all calculations was done in water solvent using cc-pvdz basis set. Fractional contributions to various fragments of the molecular orbital were obtained by GaussSum program [28].

Results and discussion

Weight loss measurements

Figure 1 shows the rates of Cu corrosion at different concentrations of DPA in 0.5 M HCl solution after 1 h of immersion at 25 °C. The corrosion rate decreases with the decrease in inhibitor concentration due to the large molecule size of DPA which is adsorbed at the metal/solution interface. The size and molecular weight of organic inhibitor also have an impact on the efficiency of inhibition [22, 29]. Larger the molecule, greater is the inhibition efficiency. Also, the corrosion rate increases when the inhibitor concentration reaches 10^{-9} M which is optimal concentration. The corrosion rate (C_R in mg cm^{-2} h^{-1}) was measured using Eqs. 1:

$$C_R = \frac{W}{A \times t} \tag{1}$$

where W (mg) is the weight loss before and after immersion in aggressive solution, A (cm^2) is the area of immersed metal coupon and t (h) is time.

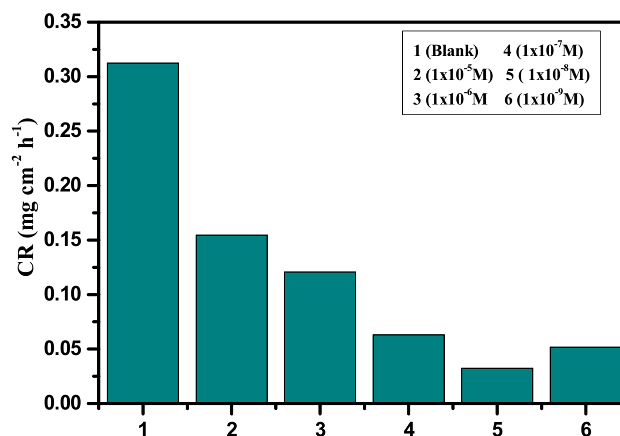

Fig. 1 Corrosion rate (CR) for copper in 0.5 M HCl solution containing different concentrations of DPA at 25 °C

Electrochemical methods

Open circuit potential

The open circuit potential of copper electrode immersed for 30 min in different concentrations of inhibitor is given in Fig. 2. In the blank 0.5 M HCl, the OCP is shifted to more positive values, which is an indicator for the formation of oxide film that attacks metal surface [30–32]. With the immersion time and with the presence of inhibitor, all OCPs are decreased toward the negative values and are stable after 30 min of immersion. The negative shift of the E_{ocp} in the presence of DPA can be explained by the adsorption of DPA on the active corrosion sites of copper surface [33, 34]. Thus, all electrochemical measurements are conducted after 30 min of immersion in 0.5 M HCl solution.

Electrochemical impedance spectroscope (EIS)

The Nyquist curves obtained during 30 min of immersion in the corrosive solution with different concentrations and without DPA at 25 °C are shown in Fig. 3a. The impedance diagrams obtained show perfect semicircles with a capacitive loop at high frequencies and a straight line (Warburg impedance) at low frequency for all Cu samples immersed in 0.5 M HCl solution with and without inhibitor. From this observation, we can conclude that copper corrosion mechanism is not affected by the addition of DPA [35, 36]. The equivalent circuit used for impedance studies is given in Fig. 3b, where R_s is a solution resistance, R_t is the charge transfer resistance, CPE (Q_d) is constant phase element and W is the Warburg impedance. The electrochemical parameters of R_t, CPE and η_z% in the presence and absence of

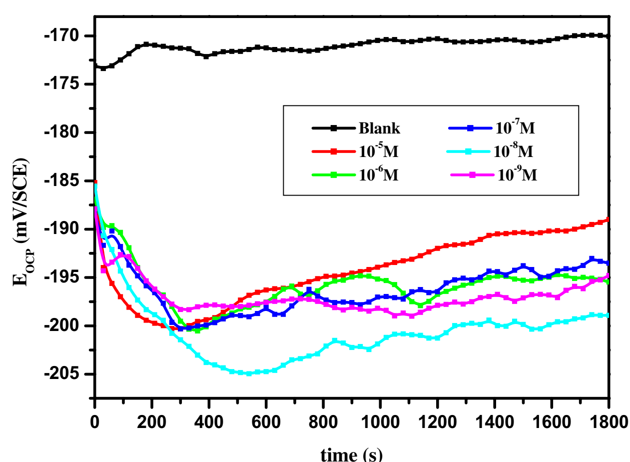

Fig. 2 Open circuit potential, E_{OCP}–time relations for copper immersed in 0.5 M HCl solution containing different concentrations of DPA at 25 °C

DPA in 0.5 M HCl are calculated by ZSimp Win software and listed in Table 1.

Table 1 shows that the values of R_t are increased, whereas the values of CPE are decreased with the decrease in DPA concentration. The values of R_t increase from 472.6 Ω cm^2 (blank) to reach the value of 4338 Ω cm^2 at 10^{-8} M of DPA. From this observation, we can imply that the metal surface is covered with a resistant film. We also notice that the values of CPE are reduced from 134.1 µF cm^2 when 10^{-8} M of DPA was used to 421.9 µF cm^2 for the blank solution. This reduction can be explained by increasing the density of the double layer and the decreasing the local dielectric constant [37, 38]. Therefore, the values of inhibition efficiency are increased with the decrease in concentration and reach the optimum values of 89% at 10^{-8} M similar to the weight loss experiments (10^{-8} M is an optimal concentration). From all these observations, we can conclude that a protective film was formed on the metal/solution interface.

The inhibition efficiency (η_z) was calculated by the charge transfer resistance values using the following Eq. (2):

$$\eta_z = \frac{R_t - R_t^{\circ}}{R_t} \times 100 \quad (2)$$

where R_t° and R_t are the charge transfer resistance in absence and in presence of inhibitor, respectively.

Potentiodynamic polarization curves

Polarization tests after 30 min in 0.5 M HCl and different concentrations of DPA at 25 °C were used to extract the corrosion potential (E_{corr}), cathodic and anodic Tafel slopes (β_c, β_a) and corrosion current density (i_{corr}), respectively. The Tafel diagrams (Fig. 4) show that the cathodic and anodic current densities are significantly decreased with the decrease in concentrations of DPA. Table 2 shows the polarization and inhibition efficiency for copper in 0.5 M HCl. The inhibition efficiency is defined by Eq. 3.

$$\eta_p = \frac{i^{\circ}_{corr} - i_{corr}}{I^{\circ}_{corr}} \times 100 \quad (3)$$

where i°_{corr} and i_{corr} are the unprotected and protected current densities of the working electrode in the 0.5 M HCl solution, respectively.

Table 2 and Fig. 4 show that the values of E_{corr}, the anodic and cathodic branches are shifted to more negative potentials as the concentration increases like the results obtained from OCP experiments. Also, there is a decrease in i_{corr} from 224.129 µA for the blank to a value of 30.814 µA and increase in the inhibitory efficiency to reach a maximum value of 89.9% when inhibitor was used indicating that the DPA forms a layer that blocks the

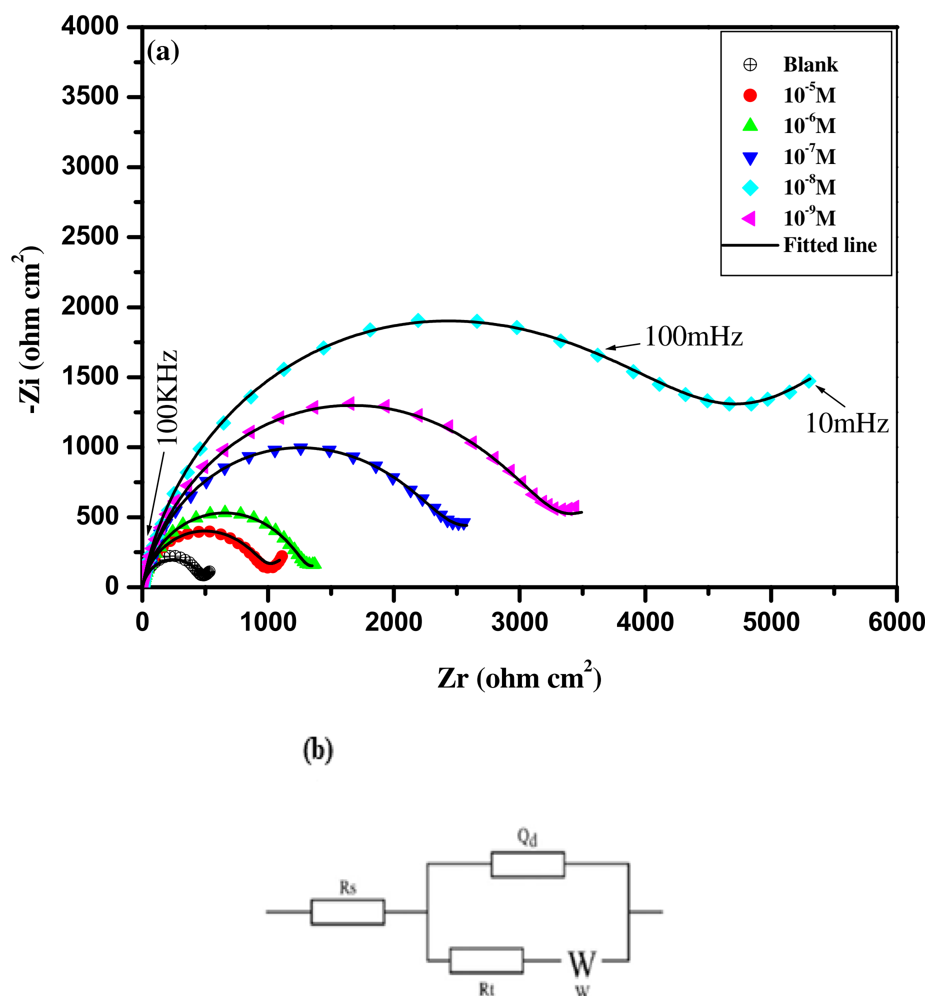

Fig. 3 Nyquist diagrams of copper in **a** 0.5 M HCl medium with or without DPA at room temperature: comparison of experimental (scatter) and fitting (red line) data and **b** electrical equivalent circuit model used to fit the experimental impedance data

Table 1 Electrochemical impedance parameters for copper in 0.5 M HCl with and without inhibitor after 30 min immersion

Conc. (M)	R_s (Ω cm^2)	CPE (μF cm^2)	n	R_t (Ω cm^2)	W (mΩ m^2)	η_Z (%)
Blank	0.5883	421.9	0.8771	472.6	28.72	–
10^{-5}	0.5495	350.7	0.8792	949.7	17.61	50.2
10^{-6}	1.001	368.7	0.8772	1276	29.48	62.9
10^{-7}	1.373	296.9	0.8702	2390	10.27	80.2
10^{-8}	2.23	134.1	0.8777	4338	2.351	89.1
10^{-9}	2.052	149.9	0.8572	3195	7.458	85.2

active sites and prevents the metal from the dissolution. The polarization data show that the addition of the inhibitor alters both β_a and β_c values. For example, the value of β_a was changed from 181.065 mV dec^{-1} for the blank to 54.003 mV dec^{-1} in the case of 10^{-8} M of DPA while for β_c, it was changed from – 293.166 to 675.612 mV dec^{-1}. The decrease in β_a and β_c values with addition of the inhibitor indicates that the DPA is a mixed-type inhibitor [39]. The efficiencies which were calculated from the weight loss, EIS and polarization methods were found to be in a good agreement.

Adsorption isotherm model study

Adsorption isotherm models can give information about the type of adsorption of DPA on metal/solution interface. Langmuir, Temkin, Frumkin, Freundlich, El-Awady and Flory–Huggins are the most frequently used adsorption isotherms. The recovery of the metal surface (θ) is obtained from the different concentrations of inhibitor using the relationship $\theta = \eta_p\%/100$ ($\eta_p\%$ is obtained from the polarization curves). The fitted linear regression coefficients (R^2) for the curves of different types of isotherms indicate that the

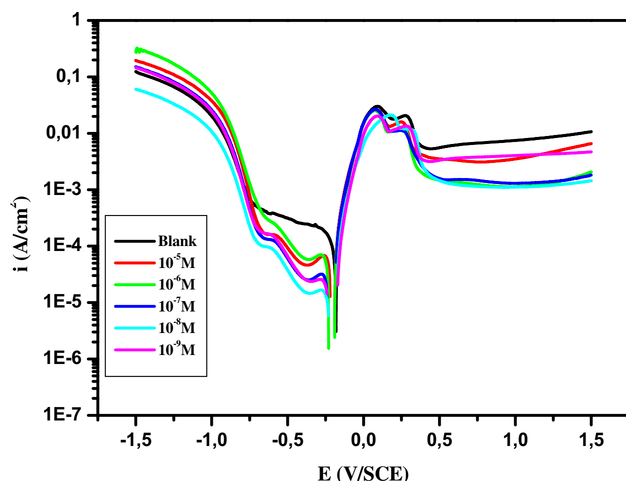

Fig. 4 Tafel curves of copper in 0.5 M HCl solutions with or without varying concentrations of DPA after 30 min

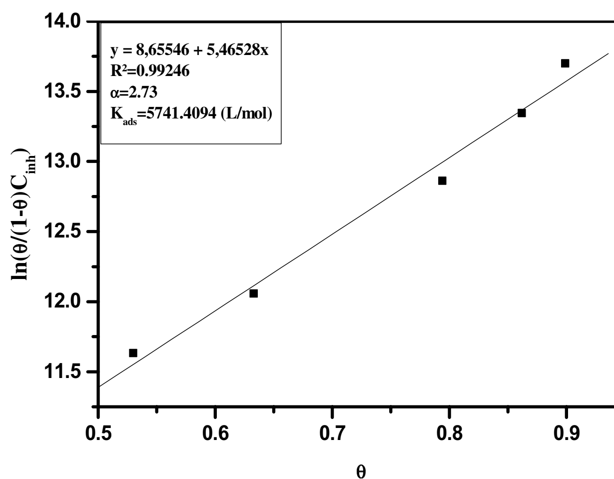

Fig. 5 The Frumkin adsorption isotherm of DPA on copper surface in the 0.5 M HCl solution at 298 K

adsorption of DPA obeys Frumkin adsorption isotherm. The Frumkin adsorption isotherm is calculated by Eq. (4):

$$\ln\left(\frac{\theta}{(1-\theta)C}\right) = lnK_{ads} + 2\alpha\theta \quad (4)$$

where θ is the degree of surface coverage, K_{ads} is the equilibrium constant of adsorption process, C is the concentration of the inhibitor and α is molecule's interaction parameters.

The results of the Frumkin adsorption isotherm model fitting are shown in Fig. 5. The value of ΔG°_{ads} is calculated from Eq. 5:

$$\Delta G^{\circ}_{ads} = -RT \ \ln \ (55.5K_{ads}) \quad (5)$$

A positive value of α (2.73) means there is an attraction for the DPA in the adsorption layer causing an increase in the adsorption energy with increase in surface coverage [37]. The measured values of K_{ads} (5741.4094 L/mol) and ΔG°_{ads} (− 31.395 kJ/mol) are presented in Fig. 5. It is well known that large K_{ads} values and small values of ΔG°_{ads} are corresponding to high corrosion inhibition performance [40, 41]. It is worthy to mention that the value of ΔG°_{ads} is negative, revealing that the DPA adsorption on the Cu surface is spontaneous. Besides, the value of ΔG°_{ads} is between − 20 and − 40 kJ/mol, revealing that the DPA adsorption on the metal surface is a combination of physical and chemical adsorption [41–43].

Effect of temperature

The current density (i_{corr}) and inhibition efficiency (η_p%) for Cu in 0.5 M HCl solution with or without varying concentrations of DPA after 30 min and in the temperature range 298–328 K were obtained from the polarization curves (Fig. 6). For all the concentrations, the i_{corr} values were found to increase with increase in temperature due to the roughness of the metal surface caused by the high temperature. It is also seen that the η_p decreases with increase in temperature, but this behavior is less pronounced at low concentrations of DPA. For example, when the concentration is 10^{-8} M, the value of η_p% varies from 89.9, 72.8, 59.3 to 39.1% as the temperature was changed from 298, 308, 318 to 328 K, indicating that covering film of the DPA on the Cu surface is stable and capable to protect the metal from the corrosion.

Table 2 Obtained data from polarization plots of copper in 0.5 M HCl at varying concentrations of DPA

Conc. (M)	E_{corr} (mV/SCE)	i_{corr} (μA cm^{-2})	β_a (mV dec^{-1})	β_c (mV dec^{-1})	R_p (Ω cm^2)	η_p (%)
Blank	− 189,467	224,129	181.065	293.166	217.136	–
10^{-5}	− 202.215	105.273	166.854	400.585	486.482	53.0
10^{-6}	− 209.070	82.105	81.421	1022.36	399.355	63.3
10^{-7}	− 207.732	46.118	66.207	527.815	554.606	79.4
10^{-8}	− 199.540	22.475	54.003	675.612	967.372	89.9
10^{-9}	− 202.215	30.814	72.787	1224.848	969.410	86.2

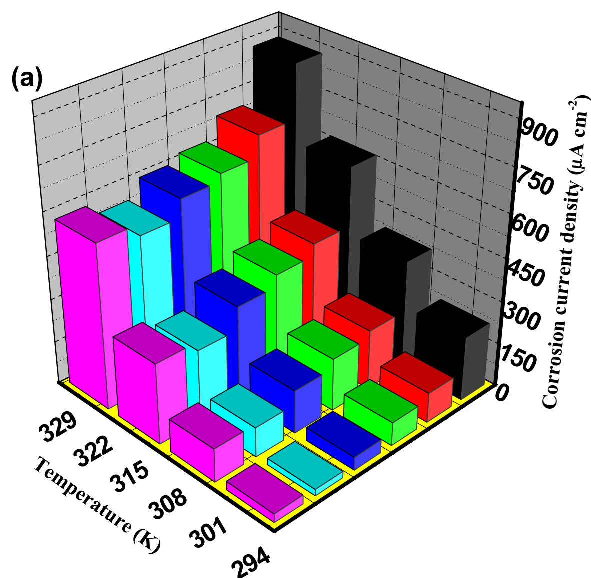

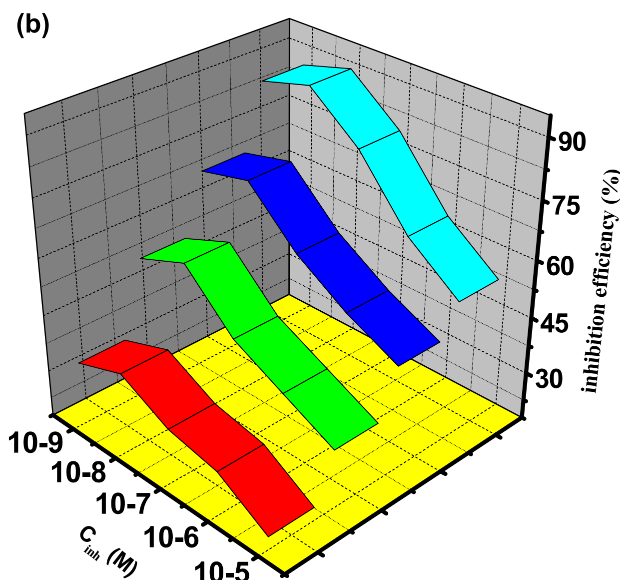

Fig. 6 **a** current density (i_{corr}) and **b** inhibition efficiency (η_p%) for copper in 0.5 M HCl solutions with or without varying concentrations of DPA after 30 min obtained from different temperatures

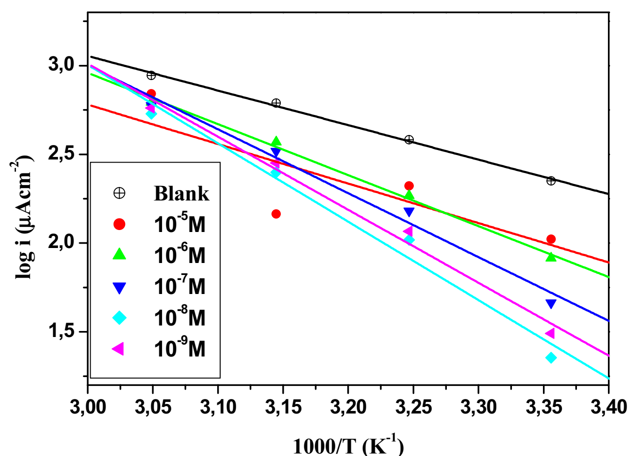

Fig. 7 Arrhenius plots for copper in 0.5 M HCl solution without and with different concentrations of DPA

Activation energy research

Thermodynamic parameters are important to understand the inhibitive mechanism. The corrosion activation energies (E_a) were calculated at different concentrations of DPA using the polarization data in 0.5 M HCl (Fig. 7). Arrhenius formula, Eqs. (6–8), was used to calculate activation parameters for corrosion process:

$$i = k\ \exp\left(-Ea/RT\right) \tag{6}$$

$$\Delta H^{\circ}_{ads} = E_a - RT \tag{7}$$

$$\Delta S^{\circ}_{ads} = \frac{\Delta H^{\circ}_{ads} - \Delta G^{\circ}_{ads}}{T} \tag{8}$$

All the calculated thermodynamic parameters are listed in Table 3.

In Fig. 7, there is a good linear relationship between logi_{corr} and 1000/T. The adsorptive equilibrium constant (K_{ads}) is decreased with the increase in temperature, demonstrating that the inhibition performance is decreased. Adsorption of DPA on the copper may modify the surface by blocking a part or all the active sites and reduce the rate of electrochemical reactions on the surface. There is an increase in E_a in presence of inhibitor which is an indication for the physical adsorption [44, 45]. The endothermic nature of the corrosion process is supported by the positive sign for ΔH°. The positive value of ΔS°_{ads} can be explained by increasing the disorder of the system due to desorption of water molecules and adsorption of inhibitor molecule on the metal surface [46–48].

The effect of immersion time

Prolonged immersion time test is necessary to find the stability of organic corrosion inhibitor. The dynamic adsorption process of DPA has been studied using EIS technique. The collected Nyquist plots for Cu electrode in 0.5 M HCl solution in the absence and presence of 10^{-8} M inhibitor with the elapsed of time at 25 °C are displayed in Fig. 8. Electrochemical impedance parameters derived from the Nyquist diagrams are listed in Table 4. Figure 8a shows that with time, the shape of the Nyquist plots is

Table 3 The activation parameters of copper in 0.5 M HCl solution containing various concentrations of DPA

Conc. (M)	R^2	K (L mol^{-1})	E_a (kJ mol^{-1})	$-\Delta G°_{ads}$ (kJ mol^{-1})	$\Delta H°_{ads}$ (kJ mol^{-1})	$\Delta S°_{ads}$ (kJ mol^{-1})
Blank	0.99	7.787E+8	16.177	60.674	13.699	0.249
10^{-5}	0.82	2.836E+9	18.491	63.877	16.013	0.268
10^{-6}	0.99	3.881E+11	23.917	76.064	21.439	0.327
10^{-7}	0.99	6.325E+13	29.930	88.683	27.452	0.389
10^{-8}	0.98	1.832E+16	36.744	102.729	34.266	0.459
10^{-9}	0.99	2.261E+15	34.208	97.545	31.730	0.433

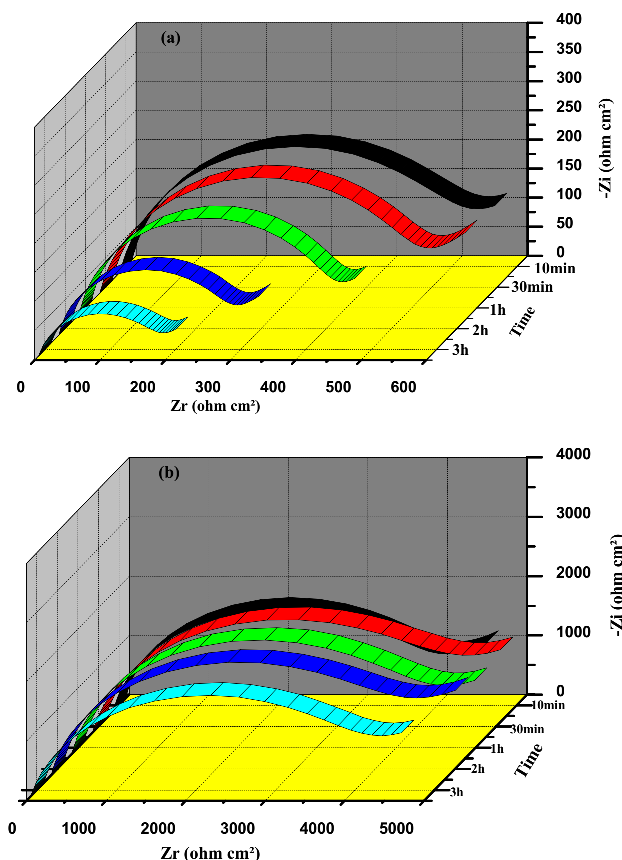

Fig. 8 Nyquist plots for copper in 0.5 M HCl solution (**a**) in the absence and presence of 10^{-8} M DPA in different immersion time at 298 K

not affected by the presence of inhibitor indicating that the mechanism of the corrosion process did not change by increasing the immersion time. For blank solution (Fig. 8a), the diameters of the semicircles of the Nyquist plots are decreased with the increase in immersion time. This indicates that in the absence of the DPA, the R_t values show exponential decrease with the exposure time. This decrease is associated with an increase in the double-layer capacitance (Table 4) because of the accumulation of corrosion products (CuCl or $CuCl_2^-$) in the diffuse double layer. The inverse proportional of R_t value with corrosion rate may be discussed on the basis that the long immersion time for copper in the acidic solution allows the hydrogen evolution kinetics to increase because the more cathodic sites are exposed by the corrosion process [49].

Whereas in the presence of 10^{-8} M DPA (Fig. 8b), R_t is decreased and η_Z is increased with the increase in immersion time which indicates that there is a stable adsorption layer of di-phosphonate derivative in copper surface.

SEM analysis and X-ray diffraction patterns

SEM images are shown in Fig. 9 for copper specimen in air (A) taken after 30 min immersion in 0.5 M HCl without (B) and with 10^{-8} M DPA (C). Clearly, the copper surface is attacked by the chloride ion leaving some small cracking after immersion in 0.5 M HCl solution (Fig. 9B) comparing to immersed one (Fig. 9A). The passivation layer formed on the copper surface is discontinuous, and it is necessary to introduce additional corrosion inhibitor to reduce the corrosion of the copper surface. Figure 9C shows that the copper surface is damaged more in the absence of inhibitor and the image shows a good protective film on the copper surface is formed from the adsorbed inhibitor species.

The X-ray diffraction patterns for the film formed on the surface of the copper specimens immersed in 0.5 M HCl with and without DPA are given in Fig. 9A′ (the pure copper specimens) and Fig. 9B′ (XRD pattern for the material in blank solution). There are different species of corrosion product of copper chloride complexes CuCl or $CuCl_2^-$ are formed on the metal surface [50–53]. In the presence of DPA Fig. 9C′, the corrosion was suppressed due to the inhibitor adsorption on the metal surface which protects surface from Cl^- attack. Consequently, XRD pattern showed the disappearance and a decrease in the intensity for some peaks due to the formation of a passivation film on copper surface. These confirm that the DPA molecules inhibit copper by forming a barrier on the surface and preventing the CuCl/$CuCl_2^-$ complex to form [50]. The XRD analysis is also in good agreement with SEM analysis and experimental results.

Table 4 Impedance parameters for copper in 0.5 M HCl without and with 10^{-8} M DPA at varied exposure time

Conc. (M)	Time	R_t (Ω cm^2)	CPE (μF cm^2)	n	R_s (Ω cm^2)	W (mΩ cm^2)	η_Z (%)
Blank	10 min	0.2886	1102	0.8762	506.6	33.17	–
	30 min	0.5883	421.9	0.8771	472.6	28.72	–
	1 h	0.3111	837.8	0.9021	377.1	56.96	–
	2 h	0.2633	1106	0.9042	241.1	48.03	–
	3 h	0.2049	2227	0.8389	178.4	75.91	–
10^{-8} M DPA	10 min	2.532	110.9	0.8956	3844	2.906	86.8
	30 min	2.23	134.1	0.8777	4338	2.351	89.1
	1 h	2.459	117.2	0.894	4302	2.606	91.2
	2 h	2.413	128.9	0.8953	4195	2.217	94.2
	3 h	2.633	161.1	0.8537	4088	3.612	95.6

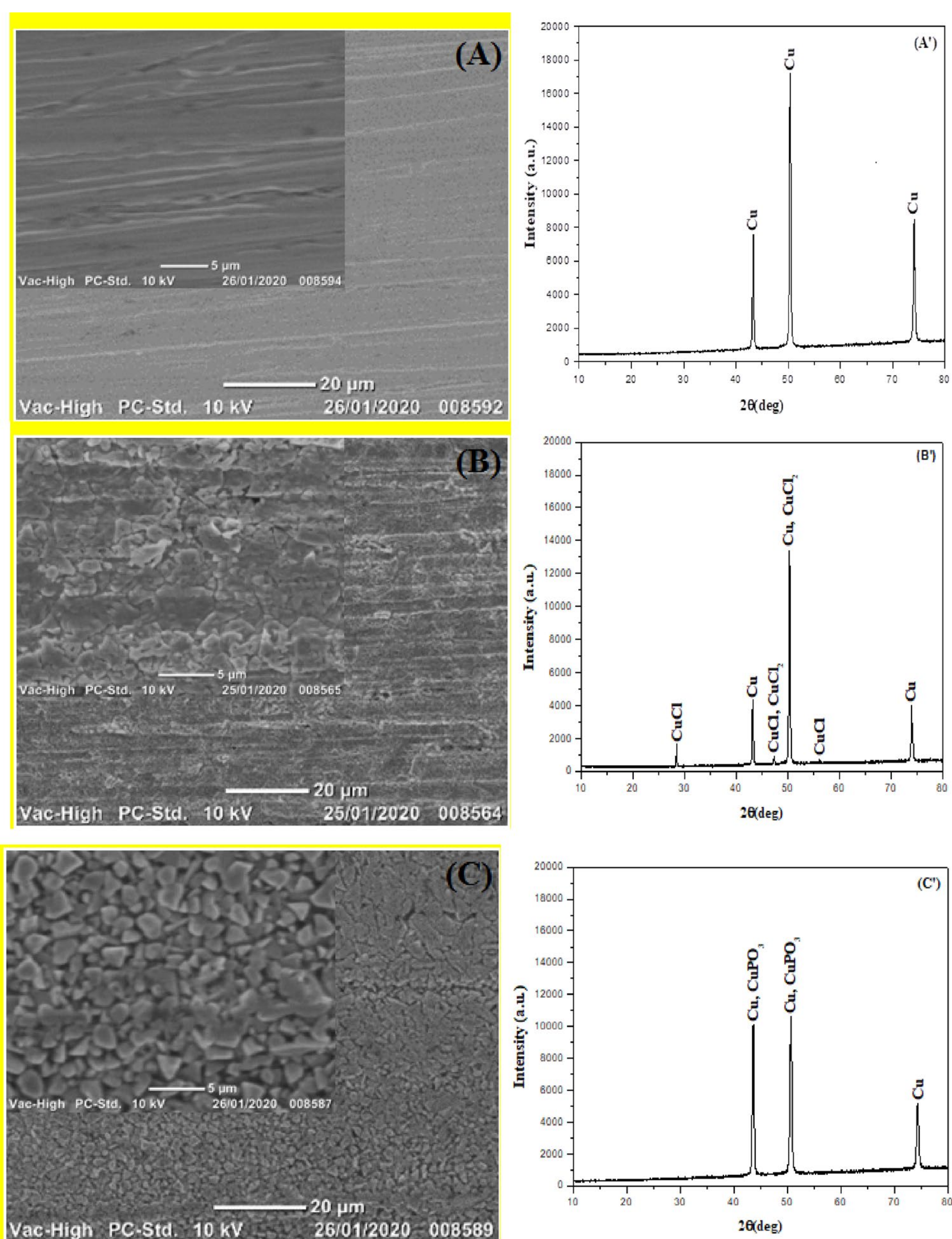

Fig. 9 SEM images and XRD patterns of the copper surface in the air (**A**, **A′**), copper surface after 30 min immersion in 0.5 M HCl (**B**, **B′**) and in presence 10^{-8} M DPA (**C**, **C′**)

Quantum chemical study of DPA

The density functional theory (DFT) is a useful technique to find the chemical parameters that are useful to explain the inhibitor/surface interaction, as well as the experimental data (Table 5). The optimized molecular structure and Mullikan charge (Fig. 10) analysis for the DPA inhibitor are used to estimate the adsorption center of adsorption of the inhibitor molecule on the metal surface [53]. Figure 10 shows that the negative regions are localized on the oxygen atoms, while positive regions are localized on the phosphorus atoms of the inhibitor molecule. This leads to a conclusion that the oxygen atoms had the strongest ability for the bonding with metal surface.

The electrostatic potential around DPA complex was calculated using the Gaussian 09 program. The atomic coordinates were extracted from the optimized structure. Blue and the red parts in the maps represent positive and negative potentials, respectively. The calculated electrostatic potential maps in Fig. 10 show that the positive and the negative centers were in asymmetric positions. Therefore, it is impossible for this inhibitor to offset its internal dipole moments. Therefore, this inhibitor showed polarity and dipole–dipole interactions, which played a significant role in forming the assembled monolayer. The HOMO gives information about the sites of the molecule that tends to donate electron to the empty orbital of the metal, while LUMO gives information about the part that accepts electron from the filled metal orbital [54]. Relative percentages of atomic contributions for the HOMO and LUMO orbitals and the isodensity plots are shown in Fig. 11. DFT results of DPA show that the HOMO is mainly phenyl ($C_6H_3CH_2C_6H_3$) in character. The LUMO molecular orbital has 61% phenyl and 30% phenolic suggesting that both the donation from π(HOMO)$\rightarrow d(Cu^0)$ and the back donation from $d(Cu^0)\rightarrow\pi^*$ (LUMO) are localized on the two-phenyl ring. As shown in Fig. 11, the charge densities of HOMO and LUMO of DPA molecule are almost uniformly distributed throughout the whole molecules. Thus, the adsorption of the inhibitor on the copper surface in a parallel mode protected copper from the corrosive medium [55].

The energy of the highest and lowest occupied molecular orbital (E_{HOMO} and E_{LUMO}) and the energy gap ($\Delta E_{gap}=E_{HOMO}-E_{LUMO}$) can be used to explain the metal/inhibitor interactions [56]. In most cases, the chemical stability of the molecule can be deduced from the energy gap (ΔE_{gap}). Lower ΔE_{gap} means adsorption of inhibitor on metallic surface is strong. The high dipole moment ($\mu=3.0115$ Debye) makes the inhibitor to form a strong dipole–dipole interaction with the metal surface. Softness

Table 5 DFT quantum parameters for DPA molecule (eV)

Inhibitor	E_{HOMO}	E_{LUMO}	ΔE	I	A	σ	χ	η	ΔN	μ (Debye)	E_{tot}
DPA	−5.36	−0.32	5.04	5.36	0.32	0.39	2.84	2.52	0.32	3.01	−1866.99

$A=-E_{LUMO}$; $I=-E_{HOMO}$; $\chi=\frac{I+A}{2}$; $\eta=\frac{I-A}{2}$; $\Delta N=\frac{\chi_{Cu}-\chi_{inh}}{2(\eta_{Cu}-\eta_{inh})}$; $\Delta E=E_{LUMO}-E_{HOMO}$; $\chi_{Cu}=4{,}48$; $\eta_{Cu}=0$

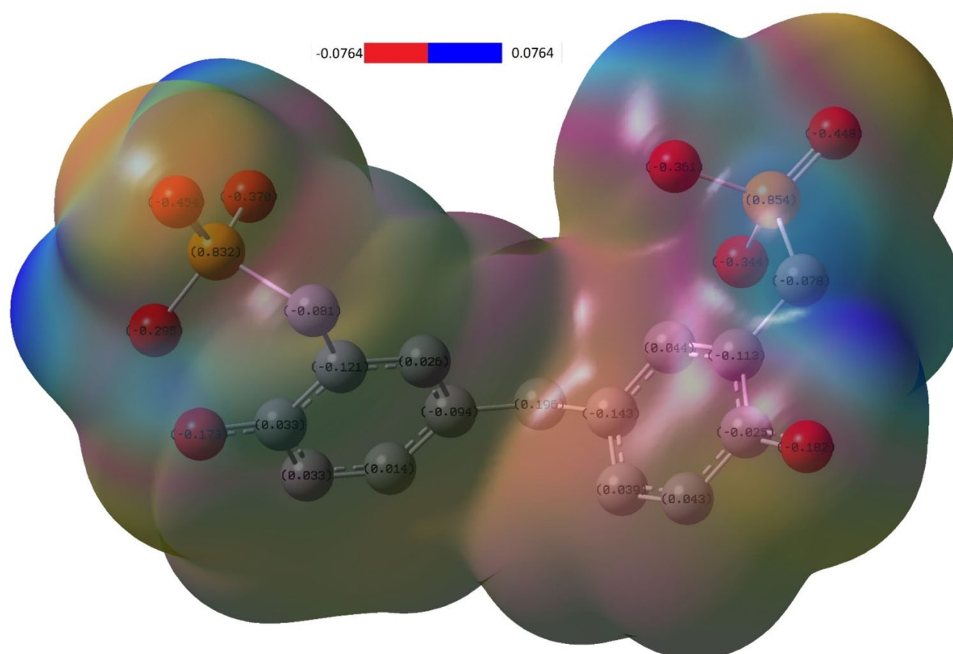

Fig. 10 The optimized structure, Mullikan charge and calculated electrostatic potential of DPA

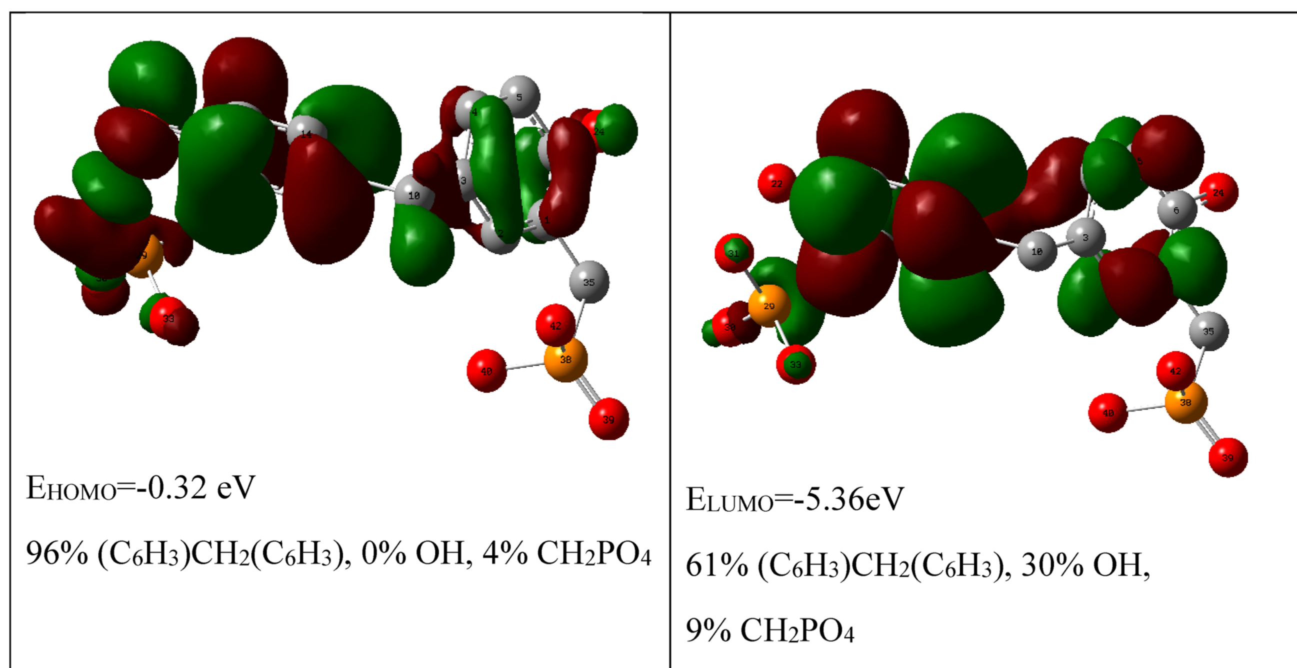

Fig. 11 Isodensity of the HOMO and LUMO orbitals of inhibitor with DFT energies and % composition of HOMO and LUMO molecular orbitals expressed in terms of composing fragments

(σ), electronegativity (χ) and hardness (η) are important parameters to estimate the stability and reactivity of the inhibitor. The high value for η (5.36), χ (2.84) and low value for σ (0.39) are both an indication for excellent inhibition efficiency. ΔN represents the fraction of electrons transferred from the inhibitor molecules to atoms of the metal upon interactions. Positive value of $\Delta N = 0.32$ demonstrates that DPA can give electrons to copper surface to form self-assembled inhibitor layers [57].

Mechanism of inhibition

From the value of ΔG°_{ads} and DFT results, we can conclude that the adsorption of the DPA on the copper surface is both physical and chemical adsorption. The physisorption can be explained as follows: Some adsorption sites of the Cu positively charged surface should be preoccupied by Cl^- present in the electrolytic solution. Because of this, there is an excessive negative charge directed to solution interface which facilitates the adsorption of protonated DPA by electrostatic interaction. The chemisorption can be explained as follows: The DPA may adsorb on the surface by the π-electron of the aromatic benzene ring and the lone pair of heteroatoms or by with the vacant d-orbital of the copper [58, 59]. The two possible modes of adsorption of DPA on Cu surface in 0.5 M HCl solution are depicted in Fig. 12.

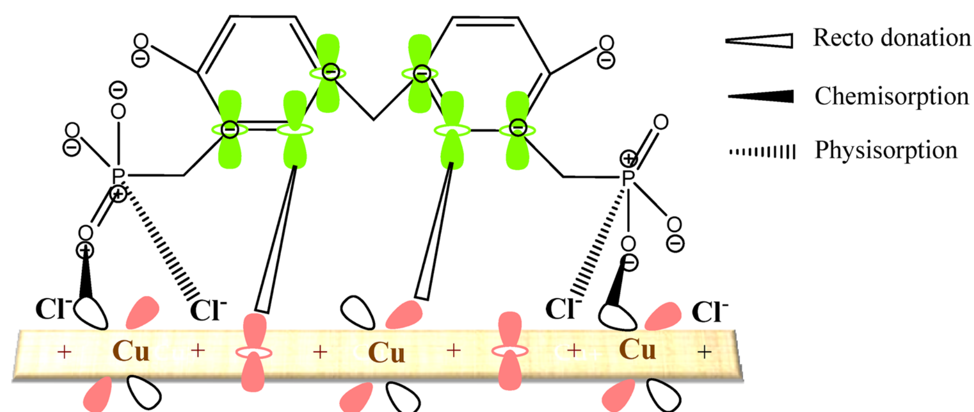

Fig. 12 Pictorial representation of adsorption of DPA inhibitor on copper surface in 0.5 M HCl

Conclusions

- Phosphonate derivative (di-phosphonic acid (DPA)) is a good inhibitor for the corrosion of copper in 0.5 M HCl medium.
- A mixed-inhibition mechanism is proposed for inhibition, and corrosion inhibition efficiency is increased with the decrease in concentration for DPA.
- Inhibitive action is due to physical and chemical adsorption of DPA on the copper surface that obey Frumkin adsorption isotherm.
- The theoretical data obtained are in a good agreement with the experimental inhibition efficiency results.
- SEM images and DRX confirm the formation of a protective layer on the copper surface.

References

1. G. Kyuchoukov, Y. Mihaylov, Hydrometallurgy **27**, 361 (1991)
2. S. Mumtaz, A. Quraishi, Corros. Sci. **70**, 161 (2013)
3. R. Farahati, H. Behzadi, S.M. Mousavi-Khoshdel, A. Ghaffarinejad, J. Mol. Struct. **1205**, 127658 (2020)
4. L. Hamadi, S. Mansouri, K. Oulmi, A. Kareche, J. Egypt Petrol. **27**, 1157 (2018)
5. A. Fateh, M. Aliofkhazraei, A.R. Rezvanian, K. Oulmi, J. Arab. Chem. **13**, 481 (2020)
6. C.J. Ing, Z. Wang, Y. Gong, H. Huang, Y. Ma, H. Xie, H. Li, S. Zhang, F. Gao, Corros. Sci. **138**, 353 (2018)
7. M.C. Bruzzoniti, R.M. De Carlo, C. Sarzanini, R. Maina, V. Tumiatti, Ind. Eng. Chem. Res. **53**, 8675 (2014)
8. M. Kabasakaloglu, T. Kiyak, O. Sendil, A. Asan, Electrochem. Appl. Surf. Sci. **193**, 167 (2002)
9. D.Q. Zhang, H. Wu, L.X. Gao, J. Mater. Chem. Phys. **133**, 981 (2012)
10. Q.J. Xu, Z.Y. Wan, G.D. Zhou, R.H. Yin, W.M. Cao, C.J. Lin, Chin. J. Chem. **26**, 1579 (2008)
11. K.M. Ismail, Electrochim. Acta **52**, 7811 (2007)
12. A.J. Isaacs, A.R. Britton, K. Mcpherson, Mater. Sci. Forum. **395**, 192 (1995)
13. R.V. Vaidya, D.P. Butt, L.E. Hersman, Corrosion **53**, 136 (1997)
14. O.P. Modi, M. Saxena, B.K. Prasad, A.K. Jha, S. Das, A.H. Yegneswaran, Corrosion **54**, 129 (1998)
15. M. Djenane, S. Chafaa, N. Chafai, R. Kerkour, A. Hellal, J. Mol. Struct. **1175**, 398 (2019)
16. S. Ramesh, S. Rajeswari, Corros. Sci. **47**, 151 (2005)
17. K.D. Demadis, E. Barouda, R.G. Raptis, H. Zhao, Inorg. Chem. **48**, 819 (2009)
18. H. Amar, J. Benzakour, A. Derja, D. Villemin, B. Moreau, T. Braisaz, Appl. Surf. Sci. **252**, 6162 (2006)
19. X.H. To, N. Pebere, N. Pelaprat, B. Boutevin, Y. Hervaud, Corros. Sci. **39**, 1925 (1997)
20. S. Rajendran, B.V. Apparao, N. Palaniswamy, V. Periasamy, G. Karthikeyan, Corros. Sci. **43**, 1345 (2001)
21. S. Saker, N. Aliouane, H. Hammache, S. Chafaa, G. Bouet, Ionics **21**, 2079 (2015)
22. D. Kameli, N. Aliouane, H. Hammache-Makhloufi, L. Makhloufi, Surf. Rev. Lett. **27**, 1950180 (2020)
23. N. Sait, N. Aliouane, N. Ait ahmed, L. Toukal, M. Al-noaimi, J. Adhes. Sci. Technol. **1**, 1 (2021). https://doi.org/10.1080/01694243.2021.1916250
24. N. Aliouane, S. Chafaa, T. Douadi, J.J. Helesbeux, M.A. Khan, O. Duval, G. Bouet, Heteroat. Chem. **2**, 51 (2010)
25. N. Aliouane, J.J. Helesbeux, T. Douadi, M.A. Khan, G. Bouet, S. Chafaa, O. Duval, Sulfur Silicon Relat. Elem. **186**, 354 (2011)
26. C. Lee, W. Yang, R.G. Parr, Phys. Rev. B **37**, 785 (1988)
27. M.J. Frisch et al., Gaussian 09, Revision D.01, Gaussian Inc, Wallingford CT, 2004 GaussView 3.0, Gaussian: Pittsburgh, PA.
28. N.M.O. Boyle, A.L. Tenderholt, K.M. Langner, J. Comput. Chem. **29**, 839 (2008)
29. M.A. Malik, M.A. Hashim, F. Nabi, S.A. Al-Thabaiti, Z. Khan, Int. J. Electrochem. Sci. **6**, 1927 (2011)
30. U.R. Evans. Edward Arnold, London. 898 (1960).
31. M.A. Amin, M.A. Ahmed, H.A. Arida, F. Kandemirli, M. Saracoglu, T. Arslan, M.A. Basaran, Corros. Sci. **53**, 1895 (2011)
32. A. Khamis, M. Saleh, M.I. Awad, Corros. Sci. **66**, 343 (2013)
33. D. Ase, M. Arami, N.M. Mahmoodi, Corros. Sci. **52**, 794 (2010)
34. A.O. Yüce, G. Kardaş, Corros. Sci. **58**, 86 (2012)
35. E.M. Sherif, S.M. Park, J. Electrochem. Soc. **152**, 428 (2005)
36. M.A. Amin, K.F. Khaled, Corros. Sci. **52**, 1194 (2010)
37. A. Döner, A.O. Yüce, G. Kardaş, Ind. Eng. Chem. Res. **52**, 9709 (2013)
38. A. Doner, G. Kardas, Corros. Sci. **53**, 4223 (2011)
39. A. Jmiai, B. El Ibrahimi, A. Tara, S. El Issami, O. Jbara, L. Bazzi, J. Mol. Struct. **1157**, 408 (2018)
40. Y. Qiang, S. Zhang, S. Xu, W. Li, J. Colloids Interface Sci. **472**, 52 (2016)
41. B. Tan, S. Zhang, Y. Qiang, W. Li, H. Li, L. Feng, L. Guo, C. Xu, S. Chen, G. Zhang, J. Mol. Liq. **298**, 111975 (2020)
42. Y. Qiang, S. Zhang, B. Tan, S. Chen, Corros. Sci. **133**, 6 (2018)
43. A. Mishra, C. Verma, H. Lgaz, V. Srivastava, M.A. Quraishi, E.E. Ebenso, J. Mol. Liq. **251**, 317 (2018)
44. C.S. Venkatachalam, S.R. Rajagopalan, M.V.C. Sastry, Electrochim. Acta **26**, 1219 (1981)
45. M.A. Quraishi, Corros. Sci. **70**, 161 (2013)
46. R. Solmaz, G. Kardaş, M. Culha, Electrochim. Acta **53**, 5941 (2008)
47. V. Branzoia, F. Branzoib, M. Baibarac, Mater. Chem. Phys. **65**, 288 (2000)
48. M.M. Saleh, Mater. Chem. Phys. **98**, 83 (2006)
49. A.M. Abdel-Gaber, Int. J. Appl. Chem. **3**, 161 (2007)
50. A. Jmiai, B. El Ibrahimi, A. Tara, S. El Issami, O. Jbara, L. Bazzi, J. Mol. Liq. **268**, 102 (2018)
51. A. Jmiai, B. El Ibrahimi, A. Tara, R. Oukhrib, S. El Issami, O. Jbara, L. Bazzi, M. Hilali, Cellulose **24**, 1 (2017)
52. E.M. Sherif, S.-M. Park, Electrochim. Acta **51**, 6556 (2006)
53. N. Khalil, Electrochim. Acta **48**, 2635 (2003)
54. L.H. Madkour, I.H. Elshamy, Int. J. Ind. Chem. **7**, 195 (2016)
55. K.F. Khaled, Corros. Sci. **52**, 2905 (2010)
56. D. Sukul, A. Pal, S. Mukhopadhyay, S.K. Saha, P. Banerjee, J. Mol. liq. **249**, 930 (2018)
57. I. Lukovits, E. Kalman, F. Zucchi, Corrosion **57**, 3 (2001)
58. N.K. Gupta, C. Verma, M.A. Quraishi, A.K. Mukherjee, J. Mol. Liq. **215**, 47 (2016)
59. N. Sait, N. Aliouane, L. Toukal, H. Hammache, M. Al-Noaimi, J.J. Helesbeux, O. Duval, J. Mol. Liq. **326**, 115316 (2021)